Available online at www.sciencedirect.com
ScienceDirect
Journal of Physics and Chemistry of Solids 67 (2006) 1965–1972
JOURNAL OF PHYSICS AND CHEMISTRY OF SOLIDS
www.elsevier.com/locate/jpcs

A multilevel hybrid optimization of magnetohydrodynamic problems in double-diffusive fluid flow

M.J. Colaço[a,*], G.S. Dulikravich[b]

[a]Department of Mechanical and Materials Engineering, Military Institute of Engineering—IME, Praça General Tibúrcio, 80—SE4, 22290-270 Rio de Janeiro, RJ, Brazil
[b]Department of Mechanical and Materials Engineering, Florida International University—EC 3474, 10555 West Flagler Street, 33174 Miami, FL, USA

Abstract

In this paper, we propose a multilevel approach based on our previously developed hybrid optimizer to solve double-diffusive fluid-flow problems in the presence of magnetic body forces. The problem consists in a square cavity subjected to a thermosolutal flow where the patterns of the isoconcentration lines are prescribed. Thus, the optimization problem is formulated in terms of the magnetic boundary conditions that must induce such a prescribed concentration profile. The optimizer is based on several deterministic and evolutionary techniques with automatic switching among them, combining the best features of each one. This code was validated against transient benchmark results for thermosolutal problems.

Keywords: D. Magnetic properties; D. Phase transitions; D. Thermodynamic properties; D. Transport properties

1. Introduction

The objective of this work is to explore the feasibility of a concept of specifying a desired pattern of concentration distribution of impurities, dopants or micro-particles in liquids undergoing thermo-circulation. For example, when growing single crystals from a melt, it is desirable that any impurities that originate from the walls of the crucible do not migrate into the mushy region and consequently deposit in the crystal. On the other hand, it is highly desirable to achieve a distribution of dopants in the crystal that is as uniform as possible [1,2]. Similarly, micro-segregation results in the interdendritic spaces when freezing a solute-enriched liquid. It does not constitute a major quality problem of the cast part, since the effects of micro-segregation can be removed during subsequent soaking and hot working. Macro-segregation, on the other hand, causes non-uniformity of composition in the cast section on a larger scale [3]. Another example is in the manufacturing of composites and functionally graded materials when it would be highly desirable to have the ability to manufacture composite parts with specified distributions of concentration of micro-fibers or nano-particles.

This de facto control of the distribution of a solute in a thermo-convective flow could be achieved by applying appropriate distributions of magnetic and/or electric fields [4] acting on the electrically conducting fluid containing the solute [5].

In this work, we will demonstrate the use of magnetic fields only. Then, the task is to determine the proper strengths, locations, and orientations of magnets that will have to be placed along the boundaries of the container so that the resulting magnetic forces will create such a thermo-convective motion of the fluid that will create the solute concentration pattern that coincides with the specified (desired) pattern of the micro-particle distribution.

Mathematical models for the combined electro-magneto-hydro-dynamics (EMHD) became available only recently [6,7]. Numerical simulation using these advanced models is still impossible because of the unavailability of the large number of physical properties that still need to be evaluated experimentally. Consequently, the complete EMHD model has traditionally been divided into two

*Corresponding author. Tel.: +55 21 2546 7264; fax: +55 21 2546 7049.
E-mail addresses: colaco@ime.eb.br (M.J. Colaço), dulikrav@fiu.edu (G.S. Dulikravich).

0022-3697/$ - see front matter © 2006 Elsevier Ltd. All rights reserved.
doi:10.1016/j.jpcs.2006.05.036

Nomenclature

B_x	magnetic flux component in x-direction
B_y	magnetic flux component in y-direction
C	concentration of the solute
C_P	specific heat at constant pressure
D	mass diffusion coefficient of the solute
g	acceleration of the gravity
Gr	Grashoff number
Gr_S	solute Grashoff number
h	enthalpy per unit mass
H	height of the cavity
k	thermal conductivity
Le	Lewis number
N	buoyancy ratio $N = Gr_S/Gr$
p	pressure
Pr	Prandtl number
Sc	Schmidt number
t	time
T	temperature
u	velocity component in x-direction
v	velocity component in y-direction
W	width of the cavity
x, y	Cartesian coordinates

Greek letters

α	thermal diffusivity
α_S	mass diffusivity
β	thermal expansion coefficient (>0)
β_S	solute expansion coefficient (<0)
μ	dynamic fluid viscosity
μ_m	magnetic permeability
σ	electric conductivity
ν	kinematic viscosity $\nu = \tilde{\mu}/\rho$
ρ	fluid density

Subscripts

0	reference value

sub-models [8,9]: (a) magneto-hydro-dynamics (MHD) that models incompressible fluid flows under the influence of an externally imposed magnetic field, while neglecting any electric fields and electrically charged particles, and (b) electro-hydro-dynamics that models the incompressible fluid flows under the influence of an externally imposed electric field, while neglecting any magnetic fields. These simplified analytical sub-models have recently been used to numerically demonstrate the feasibility of solving inverse problems in thermo-convection involving optimized magnetic and electric fields. That is, this novel manufacturing concept involves the numerical solution of MHD model and application of a constrained optimization algorithm that is capable of automatically determining the correct strengths, locations, and orientations of a finite number of magnets that will produce the magnetic field force pattern that will create the specified concentration pattern in the fluid.

2. General system of equations

The physical problem considered here involves the laminar MHD natural convection of an incompressible Newtonian fluid. The fluid physical properties are assumed constant. The energy source term resulting from viscous dissipation is neglected and buoyancy effects are approximated by the Oberbeck–Boussinesq hypothesis. Radiative heat transfer, Soret and Dufour effects are neglected. The modifications to the Navier–Stokes equations for the MHD fluid flow with heat transfer come from the electro-magnetic force on the fluid where all induced electric field terms have been neglected [6–9]. Then, the Navier–Stokes and the Maxwell equations for the MHD model can be written, for the Cartesian coordinate system as

$$\frac{\partial Q}{\partial t}+\frac{\partial E}{\partial x}+\frac{\partial F}{\partial y}=S, \tag{1}$$

$$Q=\lambda\phi, \tag{2a}$$

$$E=\lambda u\phi^{*}-\Gamma\frac{\partial\phi^{***}}{\partial x}, \tag{2b}$$

$$F=\lambda v\phi^{**}-\Gamma\frac{\partial\phi^{***}}{\partial y}. \tag{2c}$$

The values of S, λ, ϕ, ϕ^*, ϕ^{**}, ϕ^{***} and Γ are given in Table 1 for the equations of conservation of mass, species, x-momentum, y-momentum, energy, magnetic flux in the x-direction and magnetic flux in the y-direction.

Note that we used the Oberbeck–Boussinesq approximation for the variation of the density with temperature and concentration in the y-momentum conservation equation. Also note that in the energy conservation equation, the term C_PT was replaced by the enthalpy, h, per unit mass. This is useful for problems dealing with phase change where we could use the enthalpy method [10]. The above equations were transformed from the physical Cartesian (x, y) coordinates to the computational coordinate system (ξ, η) and solved by the finite volume method. The SIMPLEC method [11] was used to solve the velocity–pressure coupling problem. The WUDS interpolation scheme [12] was used to obtain the values of u, v, h, B_x and B_y as well as their derivatives at the interfaces of each control volume. The resulting linear system was solved by the GMRES method [13].

Table 1
Parameters for the Navier–Stokes and Maxwell equations

Conservation of	λ	ϕ	ϕ^*	ϕ^{**}	ϕ^{***}	Γ	S
Mass	ρ	1	1	1	1	0	0
Species	ρ	C	C	C	C	D	0
x-momentum	ρ	u	u	u	u	μ	$-\frac{\partial p}{\partial x}-\frac{B_y}{\mu_m}\left[\frac{\partial B_y}{\partial x}-\frac{\partial B_x}{\partial y}\right]$
y-momentum	ρ	v	v	v	v	μ	$-\frac{\partial p}{\partial y}-\rho g[1-\beta(T-T_0)-\beta_S(C-C_0)]+\frac{B_y}{\mu_m}\left[\frac{\partial B_y}{\partial x}-\frac{\partial B_x}{\partial y}\right]$
Energy	ρ	h	h	h	T	K	$\frac{C_P}{\sigma\mu_m^2}\left[\frac{\partial B_y}{\partial x}-\frac{\partial B_x}{\partial y}\right]^2$
Magnetic x-flux	1	B_x	0	B_x	B_x	$\frac{1}{\mu_m\sigma}$	$\frac{\partial(uB_y)}{\partial y}$
Magnetic y-flux	1	B_y	B_y	0	B_y	$\frac{1}{\mu_m\sigma}$	$\frac{\partial(vB_x)}{\partial x}$

3. Validation of the analysis code for a transient thermosolutal flow with no phase change

The MHD analysis code was validated against available analytical and experimental benchmark test cases. They involved forced convection in regular [14] and irregular channels [15], natural convection in regular and irregular cavities [16], forced convection in the presence of magnetic fields (Pouiseuille–Hartmann Flow), phase change in heat conduction and heat convection problems, natural convection in the presence of magnetic fields [17] and steady-state cooperating thermosolutal convection in enclosures [5].

In order to validate the code for the problem involving the transient cooperating thermosolutal convection in enclosures, we compared the present results with numerical results obtained by Gobin and Bennacer [18,19]. In this problem, the flow is driven by two kinds of body forces: one due to thermal buoyancy in the y-momentum conservation equation and the other due to the concentration buoyancy in the y-momentum conservation equation.

The problem considered by Gobin and Bennacer was a rectangular cavity having height H and width W as shown in Fig. 1. Different, but uniform, temperatures T_1 and T_2 and concentrations C_1 and C_2 are specified at the two vertical walls. Zero heat and mass fluxes are assumed at the top and bottom walls of the enclosure and no-slip dynamic boundary conditions are imposed at all four walls.

The following non-dimensional parameters were used in Gobin and Bennacer's work:

$$\text{Grashoff number } Gr=\frac{g\beta\Delta TH^3}{\nu^2}, \qquad \text{Prandtl number } Pr=\frac{\nu}{\alpha}, \tag{3a,b}$$

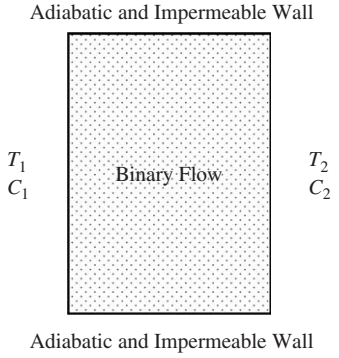

Fig. 1. Geometry and boundary conditions for the thermosolutal analysis problem.

$$\text{Solute Grashoff number } Gr_S=\frac{g\beta_S\Delta CH^3}{\nu^2}, \qquad \text{Schmidt number } Sc=\frac{\nu}{\alpha_S}, \tag{4a,b}$$

$$\text{Buoyancy ratio } N=\frac{Gr_S}{Gr}, \qquad \text{Lewis number } Le=\frac{\alpha_S}{\alpha}, \tag{5a,b}$$

where

$$\alpha=\frac{k}{\rho C_P}, \quad \alpha_S=\frac{D}{\rho}. \tag{6a,b}$$

Gobin and Bennacer [18,19] used the following parameters for their test cases involving a square cavity: $Pr=7$, $Le=100$, $Gr=4\times10^5$ and $N=20$. Since we are dealing with the conservation equations in the dimensional form, we chose the following dimensional quantities:

$$\rho=1000\,\mathrm{kg\,m^{-3}} \qquad C_P=4181.8\,\mathrm{J\,kg^{-1}\,K^{-1}}$$
$$k=0.597\,\mathrm{W\,m^{-1}\,K^{-1}} \qquad \mu=9.9933\times10^{-4}\,\mathrm{kg\,m^{-1}\,s^{-1}}$$

$\beta = 0.18 \times 10^{-3}\,\mathrm{K}^{-1}$ $D = 1.4276 \times 10^{-6}\,\mathrm{kg\,m^{-1}\,s^{-1}}$
$T_1 = 20.5\,^{\circ}\mathrm{C}$ $T_2 = 19.5\,^{\circ}\mathrm{C}$
$C_1 = 4.5\,\mathrm{kg\,m^{-3}}$ $C_2 = 5.5\,\mathrm{kg\,m^{-3}}$
$H = 305\,\mathrm{mm}$ $W = 610\,\mathrm{mm}$

The parameter β_S was calculated using Eq. (4a) in order to obtain $N = 20$ for the given parameters above. In order to obtain a cooperating thermosolutal flow, parameter β was taken less than zero, in order to obtain $N > 0$, since $\Delta T = T_2 - T_1 < 0$ and $\Delta C = C_2 - C_1 > 0$. The reference quantities T_0 and C_0 were obtained as

$$T_0 = \frac{T_1+T_2}{2}, \quad C_0 = \frac{C_1+C_2}{2}. \tag{7a,b}$$

Figs. 2 and 3 show the comparisons between the numerical results obtained using the present formulation and our software and those obtained numerically by Gobin and Bennacer for the streamlines, isotherms and iso-concentration lines at different times. In all these figures, $\Delta T = 0.05\,\mathrm{K}$ and $\Delta C = 0.05\,\mathrm{kg\,m^{-3}}$. Although the validations are only qualitative, one can notice that the results have a very good agreement, except for a little divergence in the iso-concentration lines. A possible explanation is that this minor difference arises from the fact that in Gobin and Bennacer's work, the grid had 64×64 irregularly spaced volumes, while in the present results it has 80×80 irregularly spaced volumes. The time step used in the present work was 0.005 s.

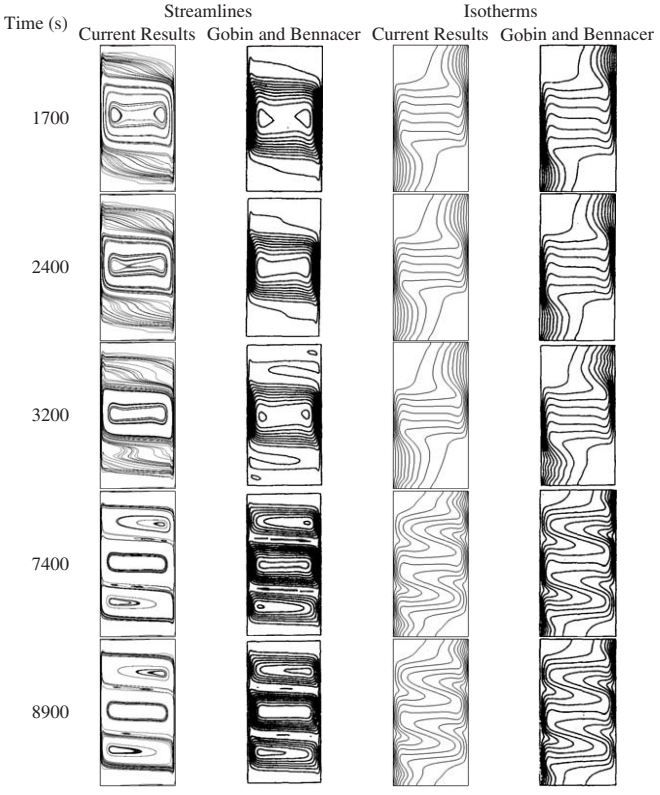

Fig. 2. Comparison between the current and Gobin and Bennacer [18,19] numerical results for the streamlines and isotherms.

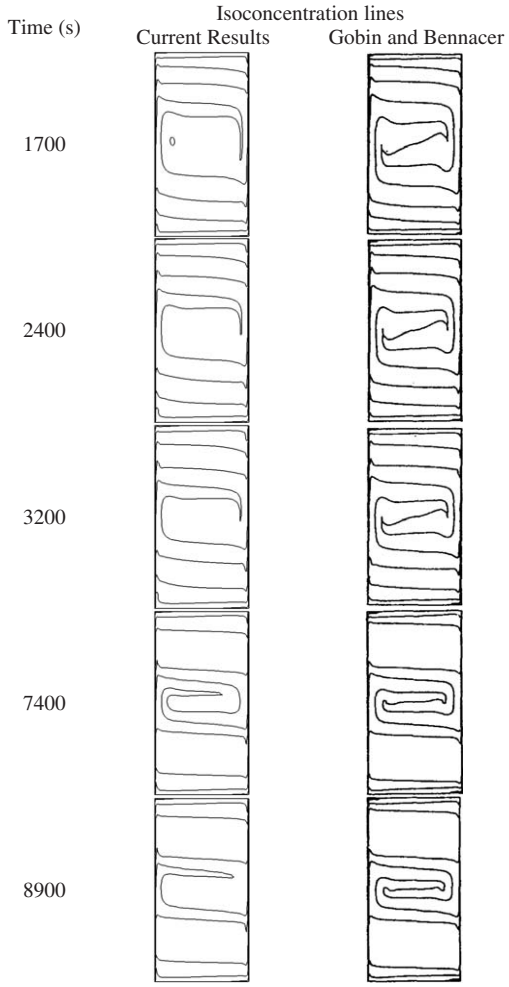

Fig. 3. Comparison between the current and Gobin and Bennacer [18,19] numerical results for the isoconcentration lines.

4. Multilevel hybrid optimizer

A hybrid optimization is a combination of the deterministic and the evolutionary/stochastic methods, in the sense that it utilizes the advantages of each of these methods. The hybrid optimization method usually employs an evolutionary/stochastic method to locate a region where the global extreme point is located and then automatically switches to a deterministic method to get to the exact point faster. The hybrid optimization method used here is quite simple conceptually, although its computational implementation is more involved. The global procedure is illustrated in Fig. 4. It uses the concepts of four different methods of optimization, namely: the Broyden–Fletcher–Goldfarb–Shanno (BFGS) quasi-Newton method [20], the particle swarm method [21], the differential evolution method [22] and the simulated annealing method [23].

In order to speed up the optimization task, a multilevel approach is utilized, where the procedure illustrated in Fig. 4 is repeated over several levels of grid refinement. Thus, the optimization procedure starts with a very coarse grid and it goes to a finer grid as the iteration continues. In

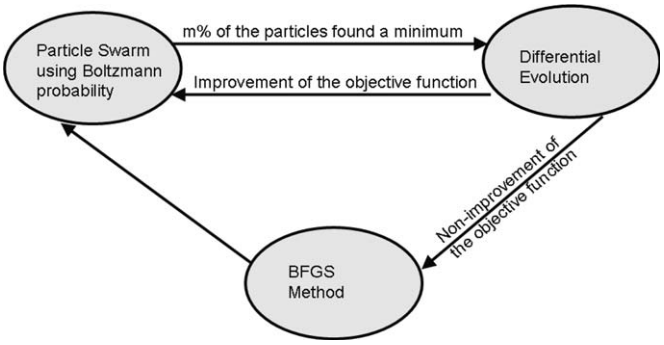

Fig. 4. Global procedure for the hybrid optimization method.

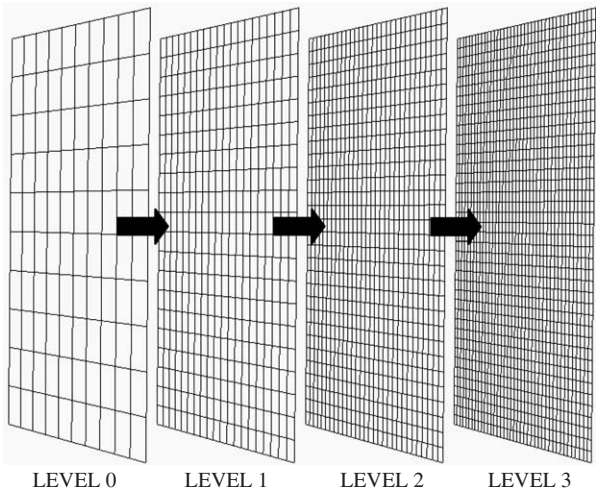

Fig. 5. A multilevel optimization sequence.

this paper, we used a four-level optimization approach. Fig. 5 shows a different grid size used in each of the optimization levels.

The driven module is the particle swarm method, which performs most of the optimization task. The particle swarm method is a non-gradient-based optimization method created in 1995 by an electrical engineer (Russel Eberhart) and a social psychologist (James Kennedy) [21] as an alternative to the genetic algorithm methods. This method is based on the social behavior of various species and tries to equilibrate the individuality and sociability of the individuals in order to locate the optimum of interest. The original idea of Kennedy and Eberhart came from the observation of birds looking for a nesting place. When the individuality is increased, the search for alternative places for nesting is also increased. However, if the individuality becomes too high, the individual might never find the best place. In other words, when the sociability is increased, individuals learn more from their neighbor's experience. However, if the sociability becomes too high, all the individuals might converge to the first place found (possibly a local minimum).

In the particle swarm method, the iterative procedure is given by

$$\mathbf{x}_i^{k+1} = \mathbf{x}_i^k + \mathbf{v}_i^{k+1}, \tag{8a}$$

$$\mathbf{v}_i^{k+1} = \alpha \mathbf{v}_i^k + \beta \mathbf{r}_{1i}(\mathbf{p}_i - \mathbf{x}_i^k) + \beta r_{2i}(\mathbf{p}_g - \mathbf{x}_i^k), \tag{8b}$$

where $\mathbf{x}_i$ is the ith individual of the vector of parameters, $\mathbf{v}_i = 0$, for $k = 0$, $\mathbf{r}_{1i}$ and $\mathbf{r}_{2i}$ are random numbers with uniform distribution between 0 and 1, $\mathbf{p}_i$ is the best value found for the vector $\mathbf{x}_i$, $\mathbf{p}_g$ is the best value found for the entire population, $0<\alpha<1$; $1<\beta<2$

In Eq. (8b), the second term on the right-hand side represents the individuality and the third term the sociability. The first term on the right-hand side represents the inertia of the particles and, in general, must be decreased as the iterative process proceeds. In this equation, the vector $\mathbf{p}_i$ represents the best value ever found for the ith component vector of parameters $\mathbf{x}_i$ during the iterative process. Thus, the individuality term involves the comparison between the current value of the ith individual $\mathbf{x}_i$ and its best value in the past. The vector $\mathbf{p}_g$ is the best value ever found for the entire population of parameters (not only the ith individual). Thus, the sociability term compares $\mathbf{x}_i$ with the best value of the entire population in the past.

The differential evolution method [22] is an evolutionary method based on Darwin's theory of evolution of the species. This non-gradient-based optimization method was also created in 1995 as an alternative to the genetic algorithm methods. Following Darwin's theory, the strongest members of a population will be more capable of surviving under a certain environmental condition. During the mating process, the chromosomes of two individuals of the population are combined in a process called crossover. During this process, mutations can occur, which can be good (individual with a better objective function) or bad (individual with a worse objective function). The mutations are used as a way to escape from local minima. However, their excessive usage can lead to a non-convergence of the method.

The method starts with a randomly generated population matrix $\mathbf{P}$ in the domain of interest. Thus, successive combinations of chromosomes and mutations are performed, creating new generations until an optimum value is found.

The iterative process is given by

$$\mathbf{x}_i^{k+1} = \delta_1 \mathbf{x}_i^k + \delta_2[\boldsymbol{\alpha} + F(\boldsymbol{\beta} - \boldsymbol{\gamma})], \tag{9}$$

where $\mathbf{x}_i$ is the ith individual of the vector of parameters, $\boldsymbol{\alpha}$, $\boldsymbol{\beta}$ and $\boldsymbol{\gamma}$ are three members of population matrix $\mathbf{P}$, randomly chosen, F is a weight function, which defines the mutation ($0.5<F<1$), k is a counter for the generations, δ_1 and δ_2 are delta Dirac functions that define the mutation.

In this minimization process, if $U(\mathbf{x}^{k+1}) < U(\mathbf{x}^k)$, then $\mathbf{x}^{k+1}$ replaces $\mathbf{x}^k$ in the population matrix $\mathbf{P}$. Otherwise, $\mathbf{x}^k$ is kept in the population matrix.

The binomial crossover is given as

$$\begin{array}{lll} \delta_1 = 0, & \text{if} & R<CR, \\ 1, & \text{if} & R>CR, \end{array} \tag{10a,b}$$

where CR is a factor that defines the crossover ($0.5 < CR < 1$) and R is a random number with uniform distribution between 0 and 1.

In the hybrid optimizer, when a certain percent of the particles find a minimum, the algorithm switches automatically to the differential evolution method and the particles are forced to breed. If there is an improvement in the objective function, the algorithm returns to the particle swarm method, meaning that some other region is more prone to having a global minimum. If there is no improvement on the objective function, this can indicate that this region already contains the global value expected and the algorithm automatically switches to the BFGS method in order to find its location more precisely. In Fig. 4, the algorithm returns to the particle swarm method in order to check if there are no changes in this location and the entire procedure repeats itself. After some maximum number of iterations is performed (e.g., five), the process stops. Details of this hybrid optimizer as well of other optimizers can be found in a recent tutorial [24].

5. Inverse problem of determining the unknown magnetic field boundary conditions

In this paper, we deal with the inverse determination of the magnetic boundary conditions that interact with thermal buoyancy and create such a fluid flow that gives some pre-specified concentration distribution of the solute within some region. Fig. 6 shows the geometry and the boundary conditions for the test cases considered here [5]. The height and length of the cavity were equal to 23 mm. The top and bottom walls were kept thermally insulated. The left boundary was kept at a "hot" temperature and low concentration of solute while the right wall was kept at a "cold" temperature and high concentration of the solute. There was no phase change, since the "hot" and "cold" temperatures were above the solidification temperature of the fluid.

The four walls were subjected to unknown magnetic field distributions whose directions were made orthogonal to each wall. In order to satisfy the magnetic flux conservation equation

$$\nabla \bullet \mathbf{B} = 0, \tag{11}$$

the following periodic conditions were imposed:

$$B_1(y) = B_2(y) \text{ and } B_3(x) = B_4(x). \tag{12a,b}$$

The objective was to minimize the natural convection effects by reducing the gradient of concentration along the y-direction, thus attempting to obtain a concentration profile similar to those obtained for pure conduction. The objective function to be minimized is therefore formulated as

$$F = \sqrt{\frac{1}{\#\text{cells}} \sum_{i=1}^{\#\text{cells}} \left(\frac{\partial C_i}{\partial y_i}\right)^2}. \tag{13}$$

The magnetic field boundary conditions were discretized at six points equally spaced along the $x = 0.0$ and along $y = 0.0$ boundaries and interpolated using B-splines for the other points at those boundaries. The magnetic boundary conditions at $x = 23$ mm and $y = 23$ mm were then obtained using periodic conditions from Eqs. (12a) and (12b).

The physical properties were taken for molten silicon [25] were used as

$\rho = 2550\,\mathrm{kg\,m^{-3}}$
$k = 64\,\mathrm{W\,m^{-1}\,K^{-1}}$
$C_P = 1059\,\mathrm{J\,kg^{-1}\,K^{-1}}$
$\mu = 0.0032634\,\mathrm{kg\,m^{-1}\,s^{-1}}$
$\sigma = 12.3 \times 10^5\,1/\mathrm{m\,\Omega}$
$\beta = 1.4 \times 10^{-4}\,\mathrm{K^{-1}}$
$g = 9.81\,\mathrm{m\,s^{-2}}$
$\mu_m = 1.2566 \times 10^{-5}\,\mathrm{T\,m\,A^{-1}}$
$Pr = 0.054.$

For the test case analyzed in this paper, we considered thermosolutal convection, with

$Gr = 10^5$
$Le = 2$
$Gr_S = 5 \times 10^5$
$N = 5.0$
$Sc = 0.108$
$D = 0.0302172\,\mathrm{kg\,m^{-1}\,s^{-1}}.$

The temperature difference $T_1 - T_2$ was set equal to 10.0 K, while the concentration difference $C_2 - C_1$ was set equal to $10.0\,\mathrm{kg\,m^{-3}}$.

Fig. 7 shows the velocity, temperature and concentration profiles predicted for this test case without any magnetic flux applied and no phase change.

Fig. 8 shows the velocity and temperature profiles resulting from six optimized terms in the B-spline on each boundary for the estimation of the magnetic boundary conditions. Under the influence of the magnetic field, the original single recirculation cell broke into two

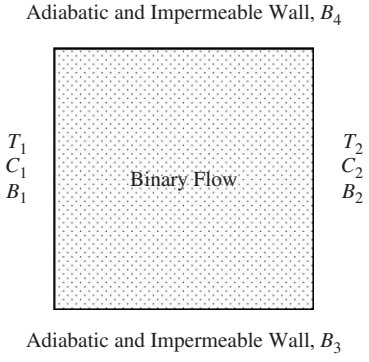

Fig. 6. Geometry and boundary conditions for MHD-controlled thermosolutal problems.

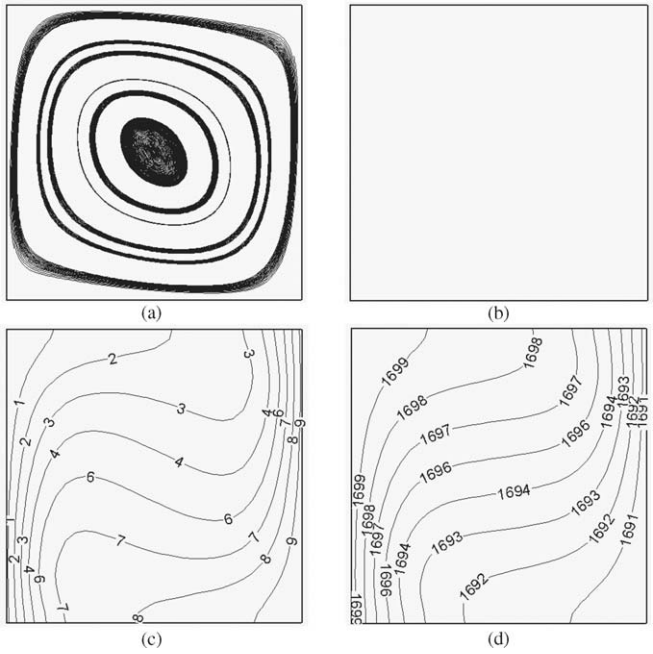

Fig. 7. Streamlines (a), magnetic flux lines (b), iso-concentration lines (c) and isotherms (d) with no applied magnetic field ($\mathbf{B} = 0$).

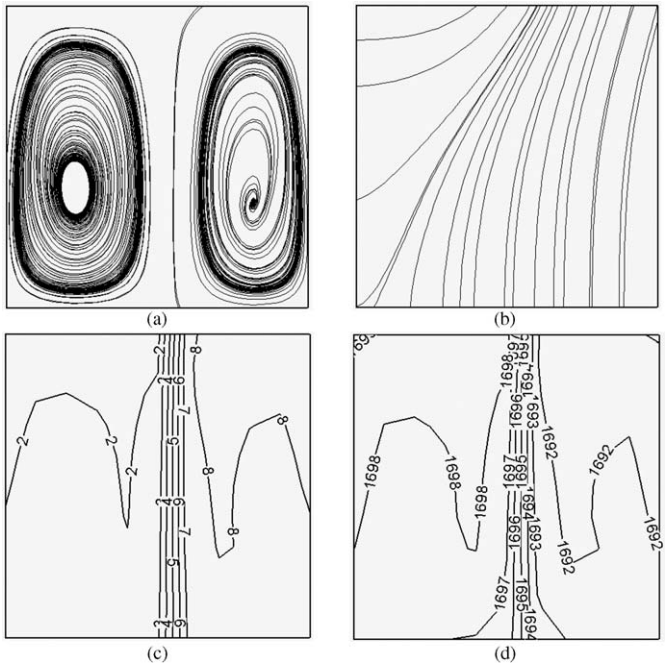

Fig. 8. Streamlines (a), magnetic flux lines (b), iso-concentration lines (c) and isotherms (d) resulting from magnetic flux **B** optimized at six points per boundary.

counter-rotating cells. One can see that the gradients of concentration in the y-direction are reduced. Using more design variables (B-spline control points) in the optimization could create better results where the gradients of concentration in the y-direction would be further reduced. It is interesting to note that since Lewis number and the buoyancy ratio N are both moderate, the curvatures of the temperature profiles are also reduced. A further investigation of the reduction of the gradients of the concentration profiles under strong thermosolutal convection is needed.

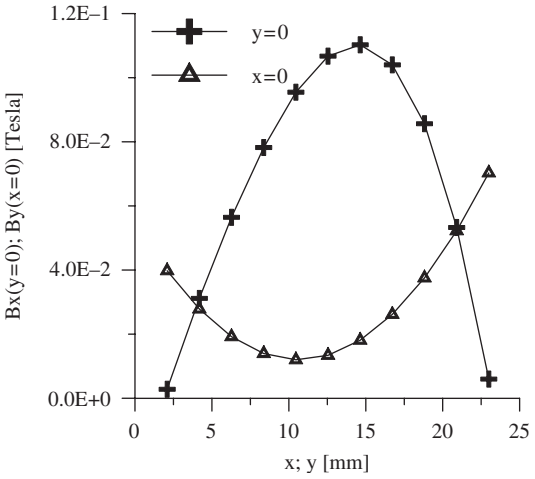

Fig. 9. Optimized magnetic boundary conditions at $x = 0$ (triangles) and $y = 0$ (crosses) with the estimation of magnetic flux **B** at six points per boundary.

Fig. 9 shows the optimized magnetic field boundary condition for $x = 0$ and $y = 0$. Notice that the strengths of the required magnetic field are very small and could be easily achieved with small permanent magnets. Fig. 10 shows the convergence history of the process of minimizing the objective function (Eq. (13)) using the hybrid optimizer with automatic switching among the optimization modules for both the Single-Level Optimization [5] and for Multi-Level Optimization. One can note that the optimum value was found quite quickly in the iterative process in this particular test case. In fact, the multilevel approach could find the optimum faster than the single level approach. In this case, only three levels (levels 0, 1 and 2 in the Fig. 5) were required. The algorithm switched the levels after 10 iterations each in this case.

6. Conclusions

In this paper, we presented the results of a transient MHD analysis code that is capable of dealing with thermosolutal problems in enclosures. The code was validated against analytical and numerical (benchmark) results showing good agreement and was applied to test cases involving steady-state optimization. The ability to minimize the natural convection effects in problems without phase change was demonstrated by determining an optimized distribution of magnetic field along the boundaries of a container. A multilevel hybrid-constrained optimization algorithm was used for reducing the concentration gradients to those similar to pure conduction problems. The multilevel optimization strategy proved to be superior to the single-level approach by reducing the

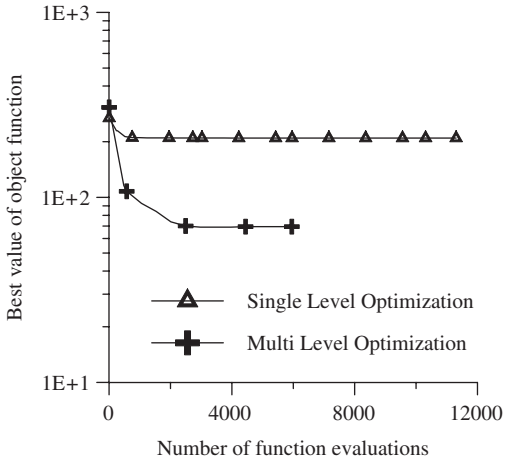

Fig. 10. Optimization convergence histories for the estimation of magnetic flux **B** at six points per boundary.

number of iterations required to reach the optimum as by finding a lower value of the objective function.

Acknowledgments

This work was partially funded by FAPERJ (agency for the fostering of science from the State of Rio de Janeiro government), CNPq (agency for the fostering of science from the Brazilian Ministry of Science) and Fundação COPPETEC (from Federal University of Rio de Janeiro). The first author is grateful also for the financial support obtained from Florida International University.

References

[1] S. Motakeff, Magnetic field elimination of convective interference with segregation during vertical-Bridgman growth of doped semiconductors, J. Cryst. Growth 104 (1990) 833–850.
[2] J.M. Hirtz, N. Ma, Dopant transport during semiconductor crystal growth: axial versus transverse magnetic field, J. Cryst. Growth 210 (2000) 554–572.
[3] A. Ghosh, Segregation in cast products, Sadhana 26 (2001) 5–24.
[4] G.S. Dulikravich, M.J. Colaco, T.J. Martin, S.-S. Lee, Magnetized fiber orientation and concentration control in solidifying composites, J. Compos. Mater. 37 (15) (2003) 1351–1366.
[5] M.J. Colaço, G.S. Dulikravich, Obtaining pre-specified concentration profiles in thermosolutal flows by applying magnetic fields having optimized intensity distribution, in: M. Papadrakakis, E. Oñate, B. Schrefler (Eds.), International Conference on Computational Methods for Coupled Problems in Science and Engineering, COUPLED PROBLEMS 2005, Santorini, Greece, 2005.
[6] G.S. Dulikravich, Electro-magneto-hydrodynamics and solidification, in: D.A. Siginer, D. De Kee, R.P. Chhabra (Eds.), Advances in Flow and Rheology of Non-Newtonian Fluids, Part B, Rheology Series, 1999 (Chapter 9).
[7] H.-J. Ko, G.S. Dulikravich, A fully non-linear model of electro-magneto-hydrodynamics, Int. J. Non-Linear Mech. 35 (4) (2000) 709–719.
[8] G.S. Dulikravich, S.R. Lynn, Unified electro-magneto-fluid dynamics (EMFD): introductory concepts, Int. J. Non-Linear Mech. 32 (5) (1997) 913–922.
[9] G.S. Dulikravich, S.R. Lynn, Unified electro-magneto-fluid dynamics (EMFD): a survey of mathematical models, Int. J. Non-Linear Mech. 32 (5) (1997) 923–932.
[10] V.R. Voller, A.D. Brent, C. Prakash, The modeling of heat, mass and solute transport in solidification systems, Int. J. Heat Mass Transfer 32 (1989) 1719–1731.
[11] J.P. Van Doormal, G.D. Raithby, Enhancements of the SIMPLE method for predicting incompressible fluid flow, Numer. Heat Transfer 7 (1984) 147–163.
[12] G.D. Raithby, K.E. Torrance, Upstream-weighted differencing schemes and their application to elliptic problems involving fluid flow, Comput. Fluids 2 (1974) 191–206.
[13] Y. Saad, M. Schultz, Conjugate gradient-like algorithms for solving non-symmetric linear systems, Math. Comput. 44 (1985) 170.
[14] M.J. Colaço, H.R.B. Orlande, Inverse problem of simultaneous estimation of two boundary heat fluxes in parallel plate channels, J. Braz. Soc. Mech. Sci. XXIII (2) (2001) 201–215.
[15] M.J. Colaço, H.R.B. Orlande, Inverse forced convection problem of simultaneous estimation of two boundary heat fluxes in irregularly shaped channels, Numer. Heat Transfer—Part A 39 (2001) 737–760.
[16] M.J. Colaço, H.R.B. Orlande, Inverse convection problems in irregular geometries, in: Proceedings of the 21st Southeastern Conference on Theoretical and Applied Mechanics, Orlando, FL, USA, 2002.
[17] G.S. Dulikravich, M.J. Colaço, B.H. Dennis, T.J. Martin, S. Lee, Optimization of intensities and orientations of magnets controlling melt flow during solidification, J. Mater. Manuf. Processes 19 (4) (2004) 695–718.
[18] R. Bennacer, D. Gobin, Cooperating thermosolutal convection in enclosures—I. Scale analysis and mass transfer, Int. J. Heat Mass Transfer 39 (13) (1996) 2671–2681.
[19] D. Gobin, R. Bennacer, Cooperating thermosolutal convection in enclosures—II. Scale analysis and mass transfer, Int. J. Heat Mass Transfer 39 (13) (1996) 2683–2697.
[20] C.G. Broyden, Quasi-Newton methods and their applications to function minimization, Math. Comput. 21 (1987) 368–380.
[21] J. Kennedy, R.C. Eberhart, Particle swarm optimization, in: Proceedings of the 1995 IEEE International Conference on Neural Networks, vol. 4, 1995, pp. 1942–1948.
[22] R. Storn, K.V. Price, Minimizing the real function of the ICEC'96 contest by differential evolution, in: Proceedings of IEEE Conference on Evolutionary Computation, vol. 1, 1996, pp. 842–844.
[23] A. Corana, M. Marchesi, C. Martini, S. Ridella, Minimizing multimodal functions of continuous variables with the 'simulated annealing algorithm', ACM Trans. Math. Software 13 (1987) 262–280.
[24] M.J. Colaço, G.S. Dulikravich, H.R.B. Orlande, T.J. Martin, Hybrid optimization with automatic switching among optimization algorithms, in: E. Onate, W. Annicchiarico, J. Periaux (Eds.), Handbooks on Theory and Engineering Applications of Computational Methods: Evolutionary Algorithms and its Applications, CIMNE, Barcelona, Spain, 2005.
[25] M.J. Colaço, G.S. Dulikravich, T.J. Martin, Control of unsteady solidification via optimized magnetic fields, Mater. Manuf. Processes 20 (3) (2005) 435–458.